Radioelectric fields from cosmic-ray air showers at large impact parameters

T. Gousset, J. Lamblin, S. Valcares

Radioelectric fields from cosmic-ray air showers at large impact parameters

Thierry Gousset, Jacob Lamblin, Sandra Valcares
Subatech – Université de Nantes, Ecole des Mines de Nantes, IN2P3/CNRS – Nantes, France

Abstract

We discuss electric fields generated by cosmic ray air showers at large impact parameters b. An approximation relevant to this situation is given. The formulation makes explicit the relationship between the shower profile and the radio pulse shapes at large b, putting forward one important observational consequence, namely the decrease of the high-frequency cutoff $\nu_c \propto 1/b^2$ when the impact parameter increases. The approximation is also used to give a detailed comparison between two emission models, the geosynchrotron model and the transverse current model.

1   Introduction

There is nowadays a renewed interest in the extensive air shower radio detection technique [1, 2]. Results have been obtained which improved on both the experimental and theoretical exploratory studies that took place during the sixties. An illuminating review of this early phase is given in Ref. [3].

From the theoretical point of view, several comprehensive frameworks have been completed or initiated in the last five years [4, 5]. The most advanced approach (geosynchrotron approach) is by Huege and collaborators [4, 6, 7]. It gives a wealth of details on the pattern of radio emission with different levels of sophistication for how the shower development is taken into account. More recently, based on the model first proposed by Kahn and Lerche [8], Scholten and Werner developed a different approach (transverse current approach) [5]. The present study can be seen as a follow-up of the latter work as it exploits a limiting behavior, the so-called *point-like approximation*, motivated in Ref. [5]. We give a somewhat different and complementary motivation for arriving at the same approximation. Our derivation follows a line of reasoning suggested in Ref. [3]. It makes it possible to extend the approximation to the cases of non vertical showers and also to get the corresponding expression for the electric field considered in Ref. [4].

We believe that, however crude the approximation may be, it might be useful in the present stage of mastering the radio detection technique when progress is made using a

delicate mix of physical prejudices and empirical facts. This is provided that the model captures some essential features of the phenomenon. For the approximation at hand a point that can be put forward is the direct relationship at large impact parameter between the time-development of an air shower and that of its radio component. This has two testable consequences. First, the decrease of the high-frequency cutoff of the electric field spectrum when the impact parameter rises: this has never been seen in experiment so far and is a crucial test for our understanding of radio emission. Next, the sensitivity of the radio component to the beginning of the shower development, making radio complementary to traditional techniques for that matter.

The derivation of the electric field expressions in the point-like approximation is given in Sect. 2 for both the transverse current and the geosynchroton approaches. This leads us to discuss the differences between the two approaches concerning on the one hand their phenomenologies and on the other hand their physical motivations. The section ends in a discussion of the domain of impact parameters and frequencies where the approximation makes sense. The relationship between the time pulse and shower evolution is investigated in Sect. 3, showing the importance of the Doppler effect. Sect. 4 is devoted to questions concerning a very large array, a natural topic for an application of large impact parameter calculations. Our main observations are collected in Sect 5.

2 The point-like model

2.1 Electric field expressions

A cosmic-ray air-shower is a charge and current system whose electromagnetic field carries genuine information on some important aspects of the shower. Because the shower front moves at about the speed of light, the electromagnetic signals emitted in the forward direction by the shower core at various stages of the shower history all travel with the particle front. Thus only at observation points located at sufficiently large impact parameters, i.e., away from the forward direction, the sequence of emissions results in a sequence of receptions, and the collected pulse is a reflection of the shower evolution. This is because the time scale *at reception* associated with the shower development becomes much larger than those coming from the shower extension. The hierarchy of time scales relevant at large impact parameters is thoroughly studied in Ref. [3].

This hierarchy suggests a model where all time scales but that due to shower evolution are set to zero. Setting time scales associated with the shower extension to zero corresponds to neglecting the shower extension altogether, hence taking the shower as a point-like system. Of course, this is only meant as a model for the densest part of the shower core where most of the ultra-relativistic charges stand. As discussed in Sect. 2.3, this model makes sense for impact parameters in the km range and at not too large frequencies.

The explicit expression for the electric field depends on both the origin of charge separation and the electric field emission mechanism. For electron-positron separation in the Earth magnetic field, two possibilities have been explored recently, considering that the
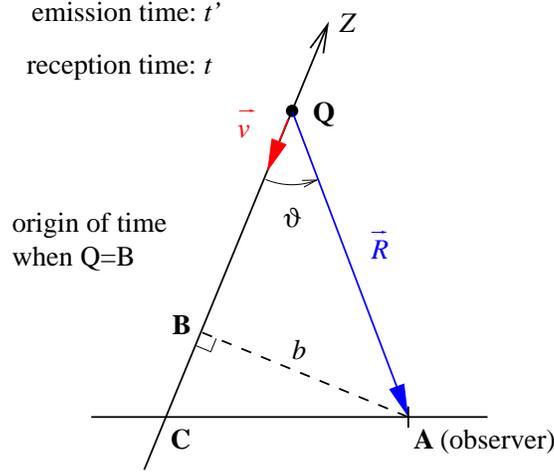
Figure 1: Geometry and notations: $\vec{R} = \overrightarrow{QA}$ and $\vartheta = \angle(\vec{v}, \overrightarrow{QA})$.

electric field is generated either by charge acceleration (geosynchrotron emission) [4] or by charge drift [5]. Both will be considered here in order to show the flexibility of our approach and to gauge the sensitivity of some results.

For a given choice of charge separation and emission mechanism the expression of the electric field in the model is essentially an adaptation of the relevant textbook formula to the case where the number of elementary charges N_{ee} evolves with time. Such a scheme was already followed in Ref. [9]. There it is also explained that at a given impact parameter b two effects are in competition for building the electric field. These are the inverse distance $1/R$ (notations in Fig. 1) between the charge and the observation point and the Doppler factor

$$\left(\frac{\partial t}{\partial t'}\right)^{-1} = \frac{1}{1 - n\beta\cos\vartheta}$$

(t' is the emission time, t is the reception time, $\vartheta = \angle(\vec{v}, \overrightarrow{QA})$, n is the refraction index and $\beta = v/c$). The larger both factors are the larger is the field. For n very close to 1 (air) and v very close to c, the Doppler factor singles out very small angles (for $n = 1$, $\vartheta = O(1/\gamma)$). The most favorable situation is therefore at small b. However, if we insist on having a somewhat larger b (so that the point-like model may apply) then the combination N_{ee}/R will single out finite angles[1] in contradistinction to the Doppler factor. The competition is illustrated in Fig. 2 as a function of Z (the relation between Z and ϑ is $Z = b/\tan\vartheta$).

As a result of the above competition, the electric field picks up its largest magnitude in a region of small but not too-small angles where the following conditions are fulfilled:

- $\vartheta \ll 1$, the Doppler contraction plays a role, so that relativistic features of radiation are partly kept,

---

[1] This is not true for very inclined showers if b is kept in the km range. For this reason inclinations were limited to $\theta \leq 60°$ in the present study.
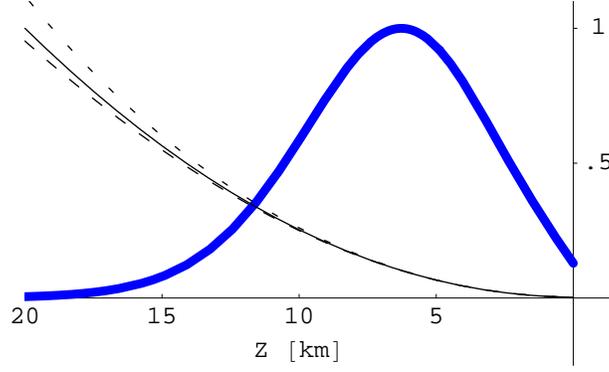
Figure 2: Shape of N_{ee}/R ($\theta = 45°$) [thick line] and that of $1/(1 - n\beta\cos\vartheta)$ ($b = 1.5$ km, $n = 1$, $\beta = 1$ [solid], $n = 1$, $\gamma = 60$ [long dashes], $n = 1.0003$, $\beta = 1$ [short dashes]).

- $\vartheta \gg \sqrt{|1 - n\beta|}$. For such angles, deviations from 1 for both the refractive index n and the particle/shower speed β are irrelevant. (See also Fig. 2.)

This is this regime which is put forward in the present study. The second item leads to approximate

$$v \approx c/n \approx c.$$

Taking the geometry shown in Fig. 1, the angle range $\vartheta \ll 1$ translates into ($\vartheta \approx \tan\vartheta = b/(-ct')$)

$$t' < 0 \quad \text{and} \quad b \ll -ct'$$

and the retarded time relation, $ct = ct' + R$, using $ct' = -b/\tan\vartheta$ and $R = b/\sin\vartheta$, leads to the following relation between t, t' and b

$$ct\, ct' \approx -b^2/2. \tag{1}$$

This greatly simplifies the computation of the electric field since all source based time dependences can be expressed as function of t and b, i.e., observer based quantities. The transverse current field reads

$$\vec{E}_v(t, A) = (N_{ee}(t') + t'\,\dot{N}_{ee}(t'))\frac{e\,\vec{v}_T}{4\pi\varepsilon_0 c}\frac{1}{(ct)^2} = \frac{e\,\vec{v}_T}{4\pi\varepsilon_0 c}\frac{4(ct')^2(N_{ee}(t') + t'\dot{N}_{ee}(t'))}{b^4}. \tag{2}$$

A complete derivation can be found in Ref. [5]. We give some details in the Appendix and also on how to arrive at the geosynchrotron field that reads

$$\vec{E}_a(t, A) = N_{ee}(t')\frac{e\,a_T\,\vec{\epsilon}}{4\pi\varepsilon_0 c^2}\frac{b^2}{2\,(ct)^3} = \frac{e\,a_T\,\vec{\epsilon}}{4\pi\varepsilon_0 c}\frac{4(ct')^2(-t'N_{ee}(t'))}{b^4}. \tag{3}$$

a_T is the transverse acceleration (transverse with respect to the shower axis) and $\vec{\epsilon}$ is a unit vector showing the polarization which is perpendicular to the shower axis and such that

$$\angle(\vec{B}_T, \vec{\epsilon}) = \frac{\pi}{2} + 2 \times \angle(\vec{B}_T, \overline{BA}). \tag{4}$$
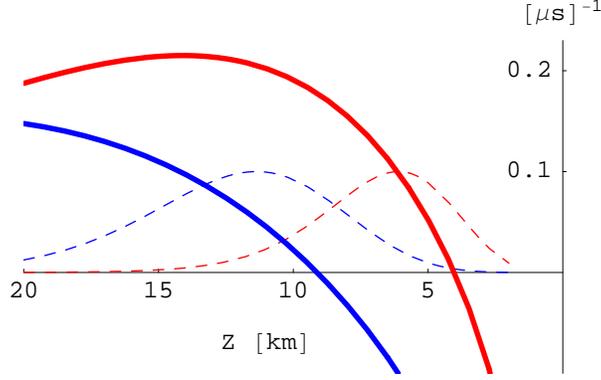
4

Figure 3: $\frac{d}{dt'}(t' N_{ee}(t'))/(t' N_{ee}(t'))$ in μs^{-1} for $\theta = 0$ (right) and $45°$ (left). Dashed curves show the respective behaviors of $E_a(t')$, rescaled so that their maxima $= 0.1$, to help focusing on the regions of interest.

In Eqs. (2) and (3), the first expressions make it easy to recognize the one-particle field approximation in the relevant ϑ range, setting $N_{ee}(t') \rightarrow$const., whereas the second expressions are useful for discussing scaling relations with b, see Sect. 2.2.

2.2   Comparisons

Eq. (2) shows that the magnitude of the field writes as a function of t' divided by b^4. As noticed in Ref. [5], because of Eq. (1) this means that the electric field pulse duration scales as b^2 and its peak value as $1/b^4$. Eq. (3) shows that the same properties hold for the geosynchrotron field.

The functional dependence on N_{ee} is different for E_v and E_a. E_a is proportional to $t' N_{ee}(t')$ whereas E_v goes like the derivative with respect to t' of this quantity. As a consequence, it is easily checked that the time integral of $\vec{E}_v(t, A)$ is zero, i.e., the E_v pulse is strictly bipolar [5]. The E_a pulse is predominantly monopolar. Sect. 3 is devoted to the discussion of the shower evolution dependence of the electric pulse.

As for comparison of magnitudes, the fields in the point-like approximation are in proportion of

$$v_T \times \frac{d}{dt'}(t' N_{ee}(t')) \text{ vs } a_T \times (t' N_{ee}(t')). \qquad (5)$$

This amounts to comparing the ratio v_T/a_T to a shower development quantity. These are genuinely different quantities, which has a consequence on their orders of magnitude, but also on their parametric dependences. Fig. 3 displays $\frac{d}{dt'}(t' N_{ee}(t'))/(t' N_{ee}(t'))$ in μs^{-1} for two zenith angles. (The ratios being time-dependent, E_a shapes are also shown to point out the relevant regions.) The estimate given in the Appendix B leads to $v_T/a_T = 0.67$ μs. Consequently, the peak value of the E_v field is one order of magnitude smaller than the E_a field. The parametric dependence of this hierarchy can be discussed by looking at the involved scales. Physically, the shower development is best described in terms of
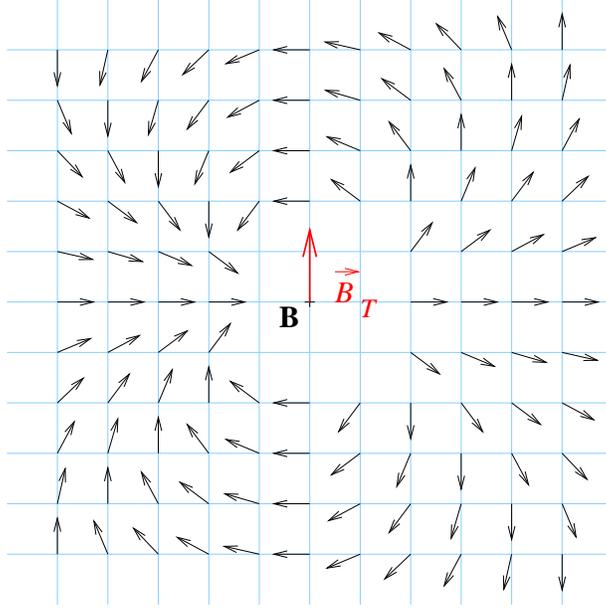
Figure 4: E_a polarization map for a shower going through the map at point B. Acceleration of positrons is to the right but the polarization is not always opposite to it. (Polarization of E_v would be to the left everywhere.)

slant depth, X, and a scale ΔX in this development, e.g., the width of $N_{ee}(X)$, can be transformed into a length scale by dividing ΔX by the air density at the point of interest, $\Delta X/\rho_{\mathrm{air}}$. The ratio $v_T/a_T \sim \tau$ is given by the lifetime of a particle (ultra-relativistic electron or positron) in the shower core [8], see also the Appendix B. Since $c\,\tau \sim X_0/\rho_{\mathrm{air}}$ the relative strength of E_v and E_a is given by the relative strength of X_0 and ΔX. The above discussed hierarchy can be seen as a consequence of $\Delta X \gg X_0$ for high-energy showers. However, no strong variation of this hierarchy was found when changing shower characteristics, such as inclination or energy.

Eq. (5) suggests that E_v and E_a are two components that derive from a single quantity. This fact may be connected to the occurrence of *angular polarization* in Ref. [3], which is the *single* quantity from which the total electric field derives in the latter formalism. In the present formulation, however, the relationship is less apparent when polarization is considered. Polarization of the velocity field is simply given by the direction of $\vec{v}_T$, i.e., perpendicular to the plan formed by the shower axis and the magnetic field. That of the geosynchrotron field, see Eq. (4) and Fig. 4, is more complex: it is still perpendicular to the shower axis, but not always in the direction of $\vec{a}_T$, hence giving another way to distinguish between E_v and E_a. The pattern shown in Fig. 4 is a purely relativistic effect. For a single charge this kind of polarization occurs at angle such that $\cos\vartheta < n\beta$, i.e., precisely the regime where the point-like approximation is formulated (see Sect. 2.1). The polarization pattern obtained in the general geosynchrotron approach is even more complex. In the

6

latter approach, at an observation point located at small b some particles are emitting at very small angles ($\cos\vartheta > n\beta$) while others are emitting at larger angles resulting in a highly non trivial pattern. However, it is possible to understand qualitatively this pattern as a superposition of a small-angle component, opposite to the acceleration, and a large angle one with the pattern shown in Fig. 4: for antennas located at the north or the south of B (we refer to the cardinal points on the map with north to the top as usual) both fields add and the result is purely EW; for points east or west of B there is a partial cancellation but the superposition remains EW; for direction NE and the like both an EW and a NS components show up. (See Fig. 3 in Ref. [6].)

As a matter of fact E_v and E_a are genuinely different. The difference has its roots in the underlying physical picture for radio emission. For the E_v field the picture is that of drifting charges much as in a conductor in a stationary state: charges are constantly accelerated by the external field but acceleration due to collisions is, on average, opposite to this external field acceleration, and coherence implies that any radiation is that of a system with no net acceleration. In the E_a approach, on the contrary, collisions are considered to be inefficient to alter the radiation associated to the external field acceleration and are disregarded (in the conductor picture this would correspond to the transient regime). A dedicated study of shower evolution is necessary in order to see which picture is the right one (or which mix is effectively relevant). Such a study, e.g., based on shower simulations, goes beyond the scope of the present work. Naively, the scales involved have a tendency to promote the drifting regime since the timescale for collision is τ which is smaller than the timescale for evolution of the shower as a whole. In the following, when limiting a study to one field, the E_v situation will be considered.

2.3 Validity

As was explained in Sect. 2.1, the point-like approximation requires that the shower evolution, *as seen by an observer*, has a time scale much larger than those due to the shower extension. The relevant time scales were studied in detail in Ref. [3] and we will essentially reproduce the reasoning here, extending the consideration to somewhat larger b and also to inclined showers.

Allan makes his estimate for a vertical shower with energy around 10^{17} eV. He first estimates a rise time for the pulse associated with the shower evolution (the so-called obliquity effect in Ref. [3]) by computing the time elapsed between the reception of a signal emitted at a height 10 km (shower "start") and that at a height 5 km (shower maximum). At small b, the shower evolution alone, i.e., the function $f_1(t') = N_{ee}(t')$, leads to the above choices for 'start' and 'max'. At larger b, Eqs. (2) and (3) show that it is rather $f_2(t') = t'^2|N_{ee} + t'\dot{N}_{ee}|$ or $f_3(t') = |t'|^3 N_{ee}(t')$ that drive the pulse behaviors. Values of $Z = -c\,t'$ at which f_1, f_2, and f_3 go through their first maxima are given in Table 1, for various inclinations and energies $E_p = 10^{19}$ and 10^{17} eV.

The rise time (multiplied by c) is, using Eq. (1),

$$\Delta_g = \frac{b^2}{2Z_{\max}} - \frac{b^2}{2Z_{\mathrm{start}}},$$

θ	max f_1	max f_2	max f_3
0	2.5	7.5	6
30	4.5	9.5	8
45	8	13.5	11.5
60	17	24.5	21

θ	max f_1	max f_2	max f_3
0	4	9	8
30	6.5	12	10
45	10.5	16.5	14
60	20.5	28.5	24.5

Table 1: $Z_{\max}$ in km: $E_p = 10^{19}$ eV (left) and $E_p = 10^{17}$ eV (right).

where Z_{start} gives an estimate for the signal start. In Allan's estimate, $Z_{\text{start}} = 2Z_{\max}$ and $\Delta_g \approx b^2/(4\,Z_{\max})$. This gives the main scaling behavior of Δ_g. More precisely, defining a starting point as the instant at which the relevant function (f_2 or f_3) reaches 10% of its maximal value, Δ_g is 90% of $b^2/(4\,Z_{\max})$ for vertical showers and 2/3 of $b^2/(4\,Z_{\max})$ for 60°-inclined showers.

Following estimates of Ref. [3] the timescale criterion for the point-like approximation reads

$$\Delta_g \gg \Delta_r = \frac{b\,r}{Z}, \qquad \Delta_g \gg \Delta_l = l,$$

where r and l are characteristic lateral and longitudinal displacements in the shower. For electrons and positrons of critical energy [3]

$$r = \frac{40 \text{ m}}{p[\text{atm}]},$$

and

$$l = \frac{3 \text{ m}}{p[\text{atm}]}.$$

The criterion $\Delta_g \gg \Delta_r$ gives $b \gg 4\,r$. For a 10^{19} eV shower, the maximum of f_2 or f_3 occurs around a 10 km height where $p = 0.3$ atm, leading to $4\,r \approx 500$ m. The second criterion, $\Delta_g \gg \Delta_l$, is equivalent to $b \gg \sqrt{4\,Z_{\max}l}$. Plugging f_2 maxima for the 10^{19} eV case gives

$$b \gg 2\sqrt{Z_{\max}l} = 0.6, 0.7, 0.8, 1 \text{ km},$$

respectively, for inclinations 0, 30, 45 et 60°. The figures show that it is the second criterion that is the most relevant.

Consideration of length scales is also important in the frequency domain. When $\Delta_g \gg \Delta_l$ and $\Delta_g \gg \Delta_r$ the loss of coherence is set by obliquity at a frequency $\nu_c \sim c/(2\pi\Delta_g)$. Since $\Delta_g \propto b^2$, an important signature of shower radio emission is provided by the observation of the scaling law $\nu_c \propto 1/b^2$ at large b. There is also an upper bound for application of the point-like approximation in the frequency domain given by $\nu_c' \sim c/(2\pi\Delta_l)$. Taking $\Delta_l = 3 - 10$ m gives $\nu_c' = 5 - 15$ MHz. These figures are also put forward in Ref. [3]. It should be noted that the experimental situation is not clear concerning the loss of coherence at small b where the scales Δ_l and Δ_r are still relevant ($\Delta_g \to 0$). It seems that a more or less flat spectrum has been observed around 50 MHz [10]. Such results call for confirmation but it may well be that the above figures for ν_c' are underestimated making

the range of applicability of the point-like model extending somewhat beyond $5-15$ MHz. In any case, observation of loss of coherence is one of the major goal to be achieved by the present radio detection experiments.

3 Deciphering the shower profile

3.1 Pulse shapes and spectra

A selection of pulse shapes and spectra is shown in Figs. 5 and 6, respectively for E_v and E_a, for showers of energy $E_p = 10^{19}$ eV and $X_{\max} = 770$ g/cm^2 and an observer at $b = 1$ km.

For E_v the beginning of the electric field pulse is polarized along $t' \dot{N}_{ee}(t') \vec{v}_T$, i.e., opposite to $\vec{v}_T \propto \hat{v} \times \vec{B}$ with $\hat{v}$ the unit vector along the shower axis and $\vec{B}$ the Earth magnetic field. For the latter we consider the situation in central Europe: the zenith angle is $\theta_B = 153°$ and the horizontal component goes from south to north. Consequently, the polarization is east-west for showers coming from north or south. Furthermore, the initial polarization is westward for a vertical shower while it is eastward for showers coming from south with $\theta \geq 27°$. This explains the various pulse signs in Fig. 5. For other shower directions, the study of polarization can be made along the same lines.

For E_a, the electric field polarization depends on the observer location with respect to the shower (see Fig. 4). Here an observer standing east or west of the shower is considered. As in the E_v case there is a flip of sign when crossing the magnetic lines at $\theta = 27°$.

The explicit relationships between pulse shape and time evolution of the shower charge number are given in Eqs. (2,3). In both cases, the Doppler-like effect, $t' \to t$, distorts the time dependence. From Eq. (1):

$$\frac{\partial t}{\partial t'} = \frac{1}{2}\left(\frac{b}{c\,t'}\right)^2 .$$

Early times (corresponding to t' negative and large) getting more contracted than later times. This explains the sharp rise, the slower decay, and in the E_v case the even slower undershoot of the pulses shown in Figs. 5 and 6.

The variation of rise time with θ was already discussed in Sect. 2.3. The probing of earlier shower stages when θ increases affects pulse shape and has the tendency to give larger fields. To get the complete change, this increase has to be combined with the overall amplitude modification coming from the variation of $\sin\alpha(\theta, \varphi)$, where α is the angle between the shower axis and the magnetic field. At fixed θ, the azimuth dependence is only through the latter overall factor. Also remember that the b dependence is simple in the approximation: pulses for another b can be deduced from Figs. 5 or 6 knowing that times are $\propto b^2$ and amplitudes are $\propto 1/b^4$.

Most of these features have of course counterparts in spectra. For the b dependence the
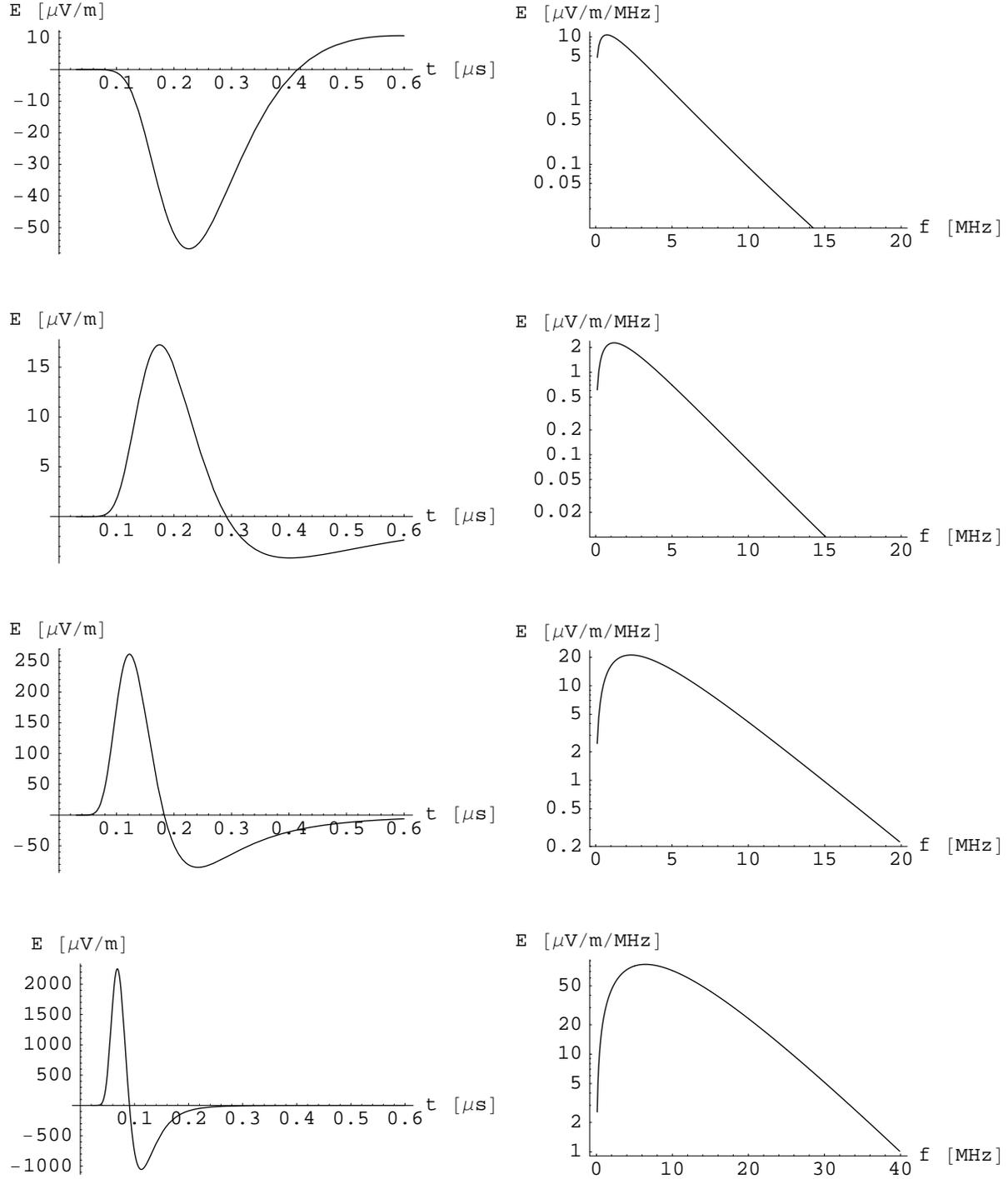
Figure 5: Transverse current electric fields at $b = 1$ km (component towards east) for showers coming from south at various zenith angles: $\theta = 0°, 30°, 45°, 60°$.
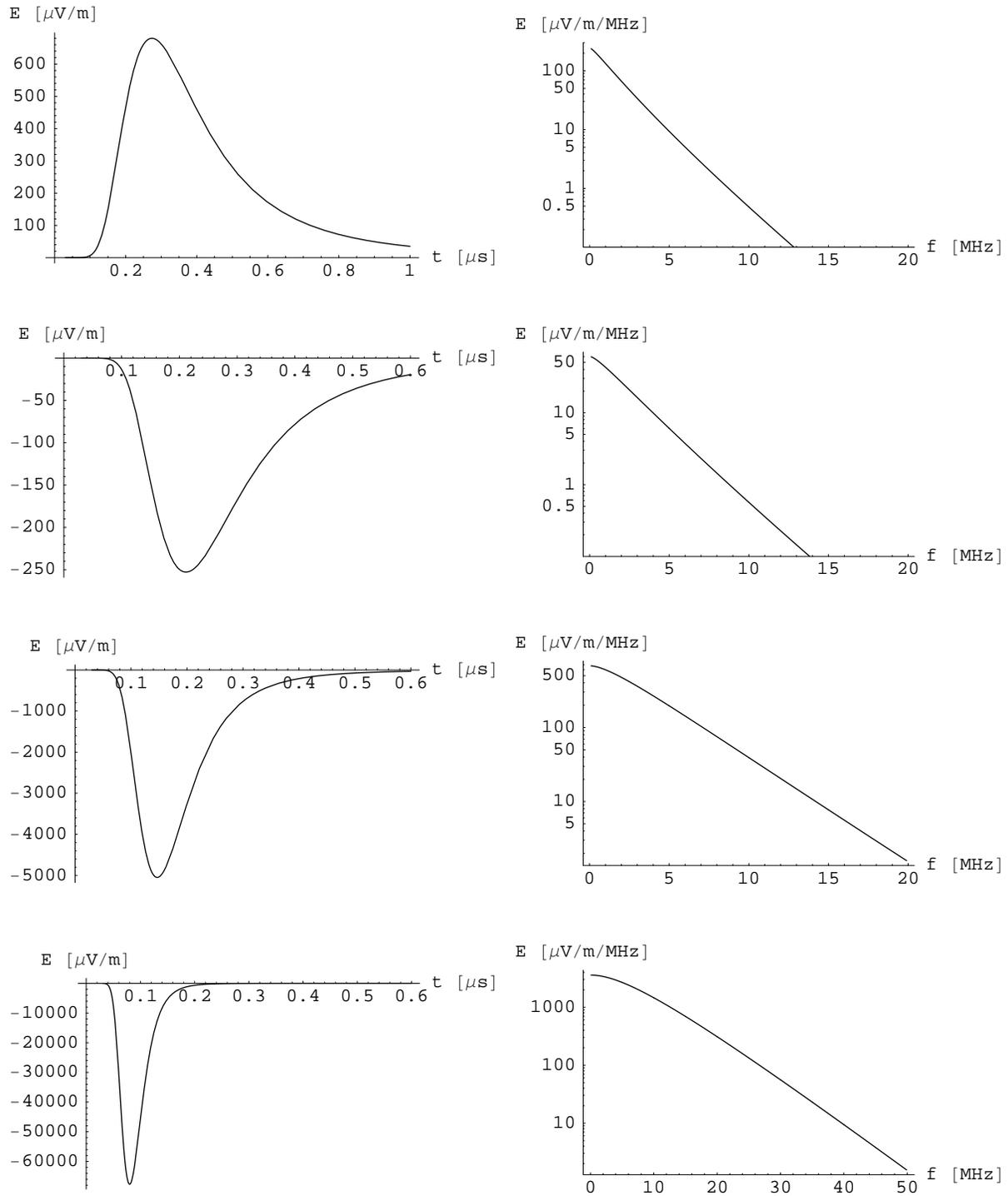
Figure 6: Geosynchrotron fields for the same configurations as in Fig. 5. The observer location is east (or west) of the shower.

11

simple form $f(t')/b^4$ for both fields Eqs. (2,3) together with Eq. (1) leads to

$$F(\nu, b) = \int dt \, \frac{f(t')}{b^4} e^{2i\pi\nu t} = \frac{1}{b^2} \int dt' \, \frac{f(t')}{2(ct')^2} e^{-i\pi\nu(b/c)^2/t'}$$

which implies that

$$F(\nu, b) = \left(\frac{b_0}{b}\right)^2 F(\nu b^2/b_0^2, b_0).$$

As for the time pulse, it is thus possible to obtain a spectrum at another b from Figs. 5 or 6 taking into account that frequencies and spectrum magnitude are both $\propto 1/b^2$. A specific application of the rescaling law for frequencies is the scaling behavior of the high-frequency cutoff, $\nu_c \propto 1/b^2$, already discussed in Sect. 2.3.

For the E_v field the spectrum is 0 at $\nu = 0$ (*bipolarity*), goes through a maximum in the MHz range for $b = 1$ km and then falls off almost as a pure exponential (*loss of coherence*) at least at not-too-large θ. At $\theta = 60°$ the loss of coherence starts beyond 10 MHz, i.e., a value comparable to the estimate given for ν'_c, reminding us that the point-like approximation is marginally applicable at $b = 1$ km for this large inclination (see Sect. 2.3). The loss of coherence for the E_a spectrum follows the same trend. The main difference is at small frequencies, the E_a spectrum being finite at $\nu = 0$.

3.2 Sensitivity to shower rise

An interesting consequence of the Doppler distortion lies in the greater sensitivity of the radio signal to the beginning of the shower. An illustration of this feature is shown in Fig. 7. The pulse height difference is a signal of the difference between the two developments (here around 8 km). The region of greater sensitivity is thus different in radio detection and in fluorescence. Note that this property is generic in radio emission at large impact parameters [9]: in the present study it was observed for both the E_v (Fig. 7) and the E_a (not shown) emission models.

The effect is more visible in the frequency domain (right plot in Fig. 7). The shower growth being pushed at larger frequencies than the shower decay by the Doppler effect, the stiffening of the time pulse for the Gaisser-Hillas profile stands out in the spectrum at large frequencies. This may be important in practice, since large radio frequency interferences often render radio observation difficult at frequencies below 20 MHz. In such circumstances the greater sensitivity of radio detection to the first stage of shower evolution may be even more pronounced.

3.3 Profile extraction

From Sect. 2.1, the electric field magnitude observed at the location of antenna i, A_i, reads

$$E_v(t, A_i) = \frac{K_v}{(ct)^2} (N_{ee}(t') + t' \dot{N}_{ee}(t')), \quad t' = \frac{-b_i^2}{2c^2 t},$$
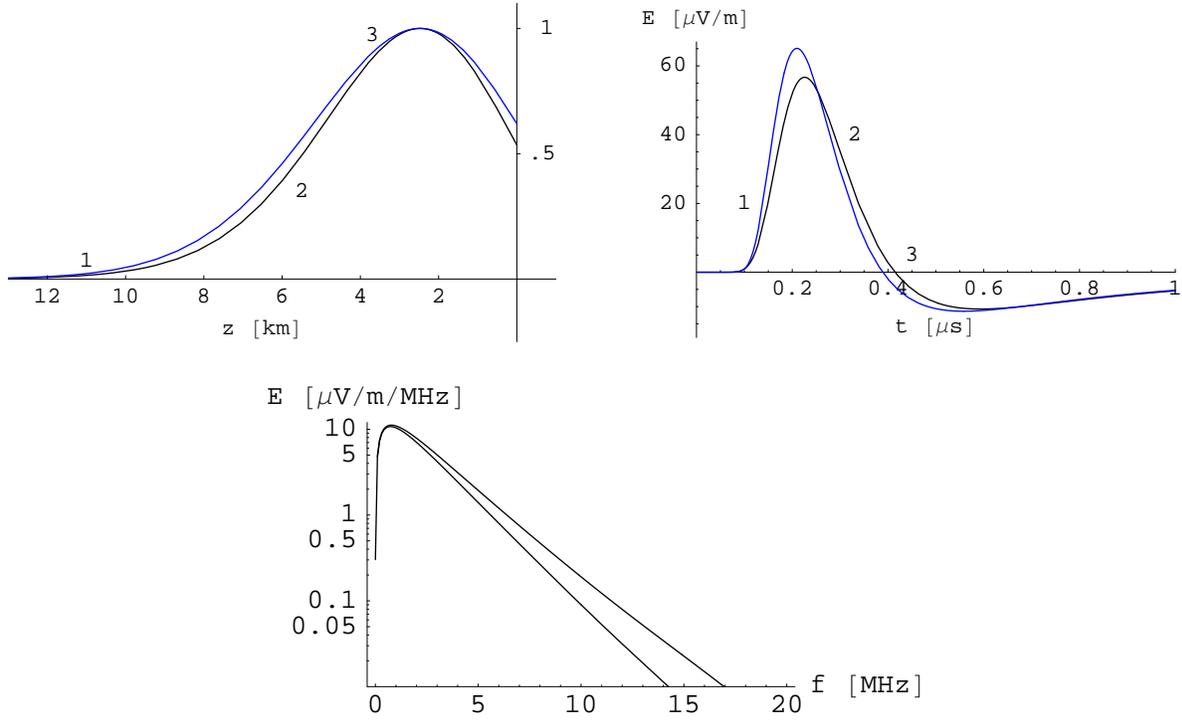
Figure 7: Sensitivity to shower rise: left plot shows two 10^{19} eV vertical-shower profiles (Gaisser-Hillas and Greisen) as a function of altitude; the corresponding E_v field pulses and spectra (at $b = 1$ km) are shown respectively on the right and bottom plots. The effect is similar for E_a (not shown).

for the transverse current component, and

$$E_a(t, A_i) = \frac{K_a\, b_i^2}{(ct)^3} N_{ee}(t'),$$

for the synchrotron one. K_v and K_a are both independent from the observation point of the event and are thus irrelevant. They can be set to 1 for the reasoning.

Such simple expressions for electric fields make it possible to illustrate what knowledge can be gained from radio measurements. Imagine the full geometry of the shower is known, i.e., both the shower incidence and the impact point location, either by some joint particle detector array or by an analysis based on radio alone [11]. Then it is possible to obtain the full time evolution of N_{ee} from the time pulse collected on antenna say $i = 1$ by looking at either

$$(ct)^2 \times E_v(t, A_1) = g_1(-b_1^2/(2ct)),$$

for the transverse current field, or

$$(ct)^3 \times E_a(t, A_1) = g_2(-b_1^2/(2ct)),$$

for the synchrotron field. In the latter case, the function $g_2(t')$ is directly proportional to $N_{ee}(t')$. In the former

$$g_1(t') = N_{ee}(t') + t'\dot{N}_{ee}(t').$$

$g_1(t')$ is the time derivative of $t'N_{ee}(t')$, so a time integration, followed by a division by t', is necessary to obtain $N_{ee}(t')$. In any case, the unfolding of the shower profile is quite simple in the model, in spite of the presence of the Doppler distortion.

In principle, the signal collected on one single antenna is enough in order to make the aforementioned extraction, but several antennas may be used to enhance the signal over background ratio. In addition, the signal can only be extracted in practice in a limited frequency-range. For sure this is the more severe limitation to the suggested analysis. However, the shower evolution is not a complete unknown and various tools of signal analysis can be considered to obtain pieces of information on the N_{ee} evolution. Having one such tool in mind, the point-like model expressions are sufficiently easy to manipulate in order to test the relevance of the foreseen method. It is not the purpose of the present study to elaborate on those methods which depend to a certain extent on the specifics of experiments and the noise situation at their locations.

4   Towards a large array

The radio detection technique is nowadays considered as a possible surrogate to more traditional techniques for future giant array, such as Auger north. One elementary detector per km^2 is the typical scale for such an array, setting the *scale* of closest approach to 1 km. Since the phenomenology discussed above applies just to this regime, it may have consequences on the exploitation of a large array which we examine here.
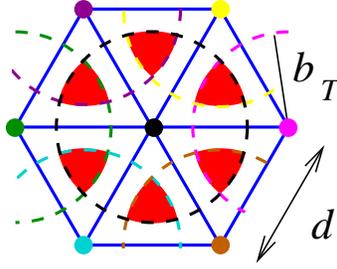
Figure 8: Hexagonal array and area of detection.

Given a detection criterion it is straightforward to count the number of antennas that see a given cosmic ray shower event, once the distribution of antennas is fixed. The geometry considered is that of an hexagonal array on a horizontal ground located at sea level and the detection efficiency is studied as a function of the antenna spacing. Our detection criterion is that the electric field magnitude is above a threshold to be defined on at least three antennas belonging to the same elementary triangle. Following Ref. [12] the threshold is first fixed to the root mean square of the galactic noise below 100 MHz (see App. D): [2]

$$E_T = \sigma_{\mathrm{sky}} = 30 \ \mu\mathrm{V/m}.$$

This is a very crude model for the detection problem but it is sufficient to demonstrate some qualitative trends. The main drawback is the assumption that the full bandwidth, and especially the low frequency range $0 - 20$ MHz, might be used for radio detection at the location of the experiment. We come back to this question at the end of the section.

A look at Fig. 5 indicates that an antenna located at 1 km receives an electric field magnitude above this threshold for a vertical shower. For such vertical events and an antenna spacing $d = 1.5$ km, Fig. 8 depicts the area spanned by impact parameters of $E_p = 10^{19}$ eV events seen by 3 antennas. The proportion of detected events is simply given by the ratio of the area of one filled region to that of a basis triangle. For 10^{19} eV vertical showers and $d = 1.5$ km this is about 35%.

The behavior of this ratio as a function of antenna spacing is given in Fig. 9, left panel, for 10^{19} eV vertical showers. The efficiency τ is a function of the impact parameter at which the threshold is reached, b_T, and the antenna spacing, d, only through the ratio of these quantities:

$$\tau \equiv \tau(d/b_T).$$

b_T appears as a natural unit for d and is in addition the value of d at which τ departs from 1. From this it is easy to see the effect of a change in the threshold level: for $E_T = 30 \ \mu\mathrm{V/m}$, $b_T = 1.15$ km; doubling E_T leads to (using $E_{\max} \propto b^{-4}$) $b'_T = 1.15/2^{1/4} = 0.97$ km.

---

[2]The assumed bandwidth is fixed by the radio experiment, i.e., not necessarily restricted to observations at large impact parameters for which the effective bandwidth is much more limited (see Sect. 3.1).
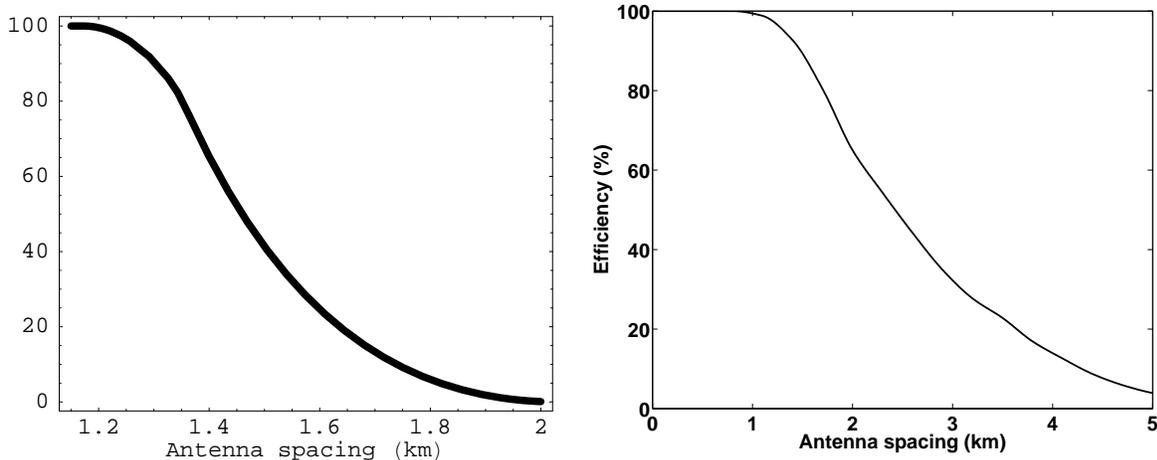
Figure 9: Detection efficiency vs antenna spacing for 10^{19} eV showers assuming transverse current emission: vertical configuration (left) and integrated over inclination (right).

It is also easy to obtain the efficiency if geosynchrotron emission is assumed. Using the figures given in Sect. 2.2 we get $b_T = 2.2$ km for $E_T = 30\ \mu V/m$. This is a large increase for the detection capability which is of course a direct consequence of the hierarchy between E_v and E_a discussed in Sect. 2.2.

The right panel in Fig. 9 displays efficiency integrated over arrival directions from vertical to $60°$-inclined showers with a weight $\sin\theta\cos\theta$, in order to incorporate changes both in solid angle and in the effective area of the antenna array. As already explained in Sect 3 (see also [9]) inclined showers are in general more effective at large impact parameters, making them easier to detect than vertical ones: for $d = 1.5$ km, the efficiency is now 90 %. This is illustrated in Fig. 10 (left panel) where the detection efficiency as a function of zenith angle in the north direction for an antenna spacing of 2 km and an energy of 10^{19} eV is presented. The effect of the zenith angle is strong. Vertical showers are never detected whereas all showers with inclination bigger than 40 degrees are detected. Of course, in practice, this would be moderated for antennas with maximum directivity pointing towards the vertical direction.

In Fig. 10, the efficiency versus azimuth for a zenith angle of 30 degrees (same antenna spacing and energy) is also shown. Fixing θ singles out the geomagnetic field effect, otherwise entangled with the zenith angle effect discussed above, since the change of efficiency in this case can only be attributed to the variation of the field strength with $\alpha(\theta, \varphi)$. The efficiency falls down when approaching the geomagnetic field direction towards the south. Here the effect is large because the choice $\theta = 30°$ is close to the magnetic lines at $27°$.

Obviously, all these results depend on shower energy. Fig. 11 shows the detection efficiency as a function of energy for an antenna spacing of 2 km, integrated over all arrival directions as in Fig. 9. The variation is not very strong as it takes three energy decades to reach 100 % efficiency.
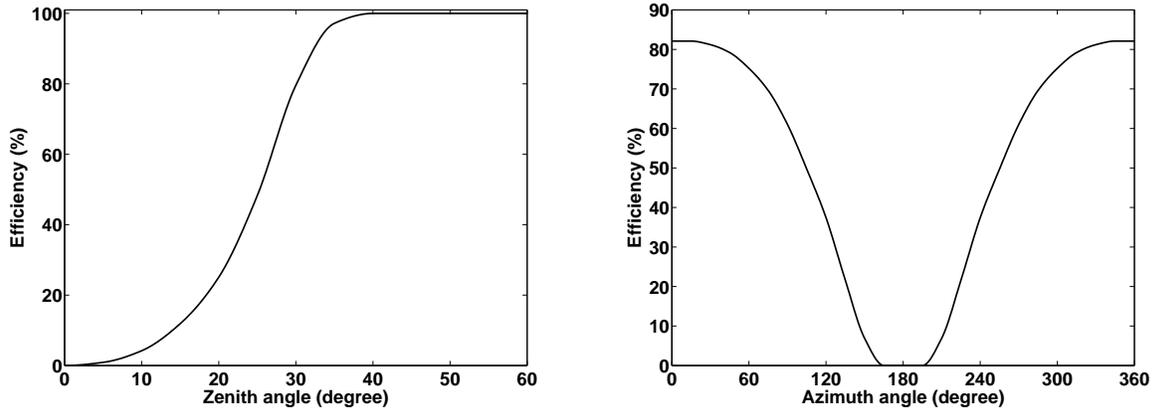
16

Figure 10: Detection efficiency assuming transverse current emission as a function of arrival direction for $E_p = 10^{19}$ eV and antenna spacing $d = 2$ km. Left: as a function of θ towards the north. Right: as a function of φ at $\theta = 30°$.
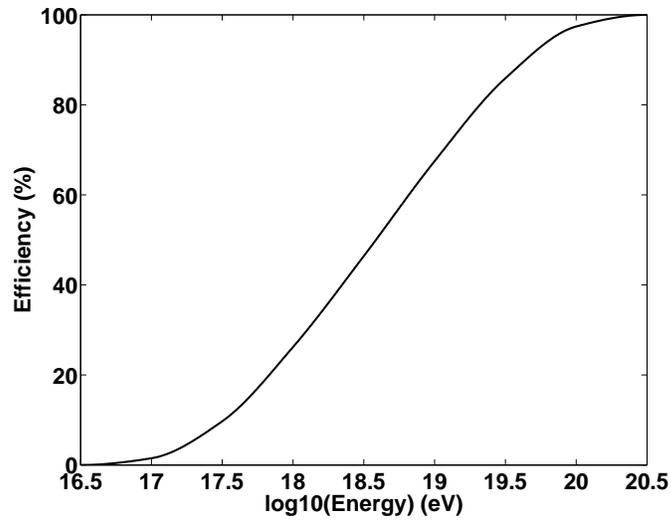

Figure 11: Detection efficiency assuming transverse current emission as a function of energy for antenna spacing $d = 2$ km.

The above detection condition requires very favorable conditions which may be approached only at exceptionally quiet location. Seemingly the site of the Pierre Auger Observatory in Malargue is of this kind, as the study of Ref. [13] shows. Even there, however, the atmospheric noise is likely to take over the galactic noise at low frequency [3]. This is not included in the computation of σ_{sky}. A dedicated study of the noise at the experimental site and as a function of time (day-night variation) would be mandatory to obtain a more realistic estimate of the background. More often, radio frequency interferences show strong variations with frequency. A detection criterion is thus best formulated in the frequency domain. In a rather quiet radio environment, a detection threshold of $1\,\mu\text{V/m/MHz}$ above 20 MHz in a $1\,\mu$s time window can be achieved [10]. Such a detection condition leads to similar results with typically a factor 0.5 on the antenna spacing. The antenna spacing for a large array should be around 1 km rather than 2 km.

5   Outlook

In the present study we showed how extensive air shower radio electric fields can be evaluated at large impact parameter with an analytical formulation. Expressions were derived for two geomagnetic effects currently under investigations in the literature, thus helping pointing out aspects for which both approaches are at variance. The relationship between radio pulse shape and shower profile, and some considerations on the sizing of a giant array could be easily discussed.

The specific figures are certainly no more than illustration, not only because the point-like approximation is too crude, but also because of their sensitivities on some shower and emission mechanism parameters. However, the approximation may be sufficient to describe tendencies and we think to make a point on some issues in the field.

As it has been understood so far in every approach to radio emission, the radio component of an air shower is driven by its time-development at large impact parameter. This is a simple consequence of propagation laws once it is assumed that the radio component is generated by the bulk of relativistic electrons and positrons in the shower. Let us collect two essential predictions that result from this fact.

The high-frequency cut in the spectrum of the shower radio-component decreases when the impact parameter increases. This prediction is not in any sense new as it was already at the heart of the discussion in Ref. [3]. Recent studies [4, 5] show specific realizations of this universal phenomenon. Only in the point-like model developed here, it is easy to isolate the origin of the phenomenon and because of its universal nature to emphasize the need to look for it. As a byproduct, we stressed that triggering at high frequency has the consequence of biasing radio detection towards small impact parameter and thus making the corresponding device blind to the phenomenon. We also emphasized that the interrelation between impact parameters and accessible frequency range is one of the main topic to be addressed when designing a large radio detection array.

The radio signal is sensitive to the beginning of the shower development, much more so than the fluorescence signal is whose sensitivity is directly proportional to N_{ee}. Thus radio

is complementary to the fluorescence technique for the purpose of measuring the shower development. Such a sensitivity may help to discriminate between various high-energy hadronic scenarios, hence providing a rich potential for the radio technique.

Acknowledgments

A Derivation of electric fields in the point-like approximation

A.1 Point-Like expressions

For a point-like charge,

$$\rho(t, \vec{x}) = q\delta^{(3)}(\vec{x} - \vec{v}t), \quad \vec{j} = \rho\vec{v}$$

a direct application of Maxwell equations in a medium of refractive index n leads for the scalar and vector potentials in Lorentz gauge to

$$V(t, \vec{x}) = \frac{1}{4\pi\varepsilon_0 n^2} \frac{q}{R|1 - n\,\vec{v}\cdot\vec{n}/c|}, \quad \vec{A}(t, \vec{x}) = \frac{1}{4\pi\varepsilon_0 c^2} \frac{q\vec{v}}{R|1 - n\,\vec{v}\cdot\vec{n}/c|},$$

with $\vec{n} = \vec{R}/R$.

For an accelerating charge, the derivation of the acceleration field is in textbooks. A positron and an electron at the same location and with the same speed have opposite accelerations and therefore produce the same electric field. Then, in the point-like approximation, N_{ee} positrons and electrons generate

$$\vec{E}_a = N_{ee}\frac{e}{4\pi\varepsilon_0 c^2} \frac{\vec{n} \wedge \left[(\vec{n} - n\vec{v}/c) \wedge \vec{a}\right]}{R|1 - n\,\vec{v}\cdot\vec{n}/c|^3},$$

where $\vec{a}$ is the positron acceleration.

For E_v, the derivation from the potentials with a time varying charge $q \to N_{ee}(t') \times e$ leads to (see also [5])

$$\vec{E}_v = N_{ee}\frac{e\vec{v}_T}{4\pi\varepsilon_0 nc} \frac{n^2 v^2/c^2 - \vec{v}\cdot\vec{n}/c}{R^2|1 - n\,\vec{v}\cdot\vec{n}/c|^3} - \dot{N}_{ee}\frac{e\vec{v}_T}{4\pi\varepsilon_0 c^2} \frac{1 - n\,\vec{v}\cdot\vec{n}/c}{R|1 - n\,\vec{v}\cdot\vec{n}/c|^3},$$

where $\vec{v}_T$ is the positron drift velocity.

A.2 Small angle approximation

A further simplification is motivated in Sect. 2.1, relevant in the region of small angles such that

$$\sqrt{|1 - n\,v/c|} \ll \vartheta \ll 1.$$

Applying this simplification to the above electric field expressions makes use of the following set of rules

$$R \rightarrow b/\vartheta, \qquad 1 - n\,\vec{v}\cdot\vec{n}/c \rightarrow \vartheta^2/2, \qquad \vartheta \rightarrow 2\,ct/b.$$

The numerator of $\vec{E}_a$ is given by

$$\vec{n} \wedge \left[(\vec{n} - nR\vec{v}/c) \wedge \dot{\vec{v}} \right] \approx \frac{\vartheta^2}{2}\left(2(\hat{b}\cdot\vec{a}_T)\hat{b} - \vec{a}_T\right) \equiv \frac{\vartheta^2}{2}a_T\vec{\epsilon},$$

where $\vec{a}_T$ is the acceleration transverse to $\vec{v}$, or equivalently to $\vec{n}$ since this is the same at small ϑ. These replacements (together with $n\,v/c \rightarrow 1$) lead to Eqs. (2) and (3).

B   Acceleration and drift velocity

In order to get quantitative values for the electric fields we need estimates for a_T and v_T which we collect from various sources in the literature. For a shower whose axis makes an angle α with the geomagnetic field $\vec{B}$, the acceleration of an electron or a positron in the shower core is $ecB\sin\alpha/(\gamma m_e)$. Averaging this over γ ($1/\bar{\gamma} = \langle 1/\gamma\rangle$) leads to an estimate for a_T in Eq. (3)

$$a_T = \frac{ecB\sin\alpha}{\bar{\gamma}m_e}.$$

Taking $\bar{\gamma} = 60$, which corresponds to the median value [3] and to a mono energetic approximation in Ref. [4], thus enabling us to make contact with computation there, together with $B\sin\alpha = 20\ \mu$T we get

$$a_T/c = 0.06\ \mu\text{s}^{-1}.$$

After time t the electron or positron has a transverse velocity $(1/\gamma m_e)ecB\sin\alpha\,t$. Kahn and Lerche [8] use this with replacements $t \rightarrow \tau = 1\ \mu$s ($\tau$ is the lifetime of the particle in the shower) and $\gamma \rightarrow \bar{\gamma}$. With $\bar{\gamma} = 60$, this gives $v_T/c = 0.06$.[3] A detailed approach to more properly estimate the drift velocity taking into account both energy loss and energy dependence of the lifetime τ is given in Ref. [5]. It leads to

$$v_T/c = 0.04,$$

and this is the value which is used in the present paper for vertical showers.

---

[3]In Ref. [8], $\bar{\gamma} = 200$ is quoted, which would lead to $v_T/c = 0.02$.

C Shower characteristics

For shower evolution we primarily used the Greisen parametrization [14]

$$N(X) = \frac{0.31\, E_p/E_C}{\sqrt{\ln E_p/E_C}} \exp\left[(X - X_{\max} - \frac{3\,X}{2}\ln s)/X_0\right], \quad s = \frac{3X}{X + 2X_{\max}},$$

with $E_C = 89$ MeV and $X_0 = 36.7$ g/cm^2. Throughout, $X_{\max}$ was chosen as 770 g/cm^2 (respectively 700, 630) for $E_p = 10^{19}$ eV (respectively 10^{18}, 10^{17}) [5].

For comparison, the Gaisser-Hillas parametrization [15] was also considered

$$N(X) = \frac{0.31\, E_p/E_C}{\sqrt{\ln E_p/E_C}} \left(\frac{X}{X_{\max}}\right)^{X_{\max}/\lambda} \exp - \left(\frac{X - X_{\max}}{\lambda}\right), \quad \lambda = 70 \text{ g/cm}^2.$$

In addition, the observation level was always chosen as that of sea-level and the atmosphere thickness as a function of altitude, for a shower coming from the direction of zenith angle θ, was taken as

$$X(z, \theta) = \frac{1020 \text{ g/cm}^2}{\cos\theta} \exp(-z/(8.8 \text{ km})).$$

D Detection threshold

To be visible a shower radio signal should be above the contribution from the galactic noise, whose power spectral density (for one polarization) is given by [16]

$$P_\nu = k_B T_{\text{sky}}(\nu).$$

This can be related to the electric field ϵ_ν to which an antenna with gain G (effective area $A_e = G\lambda^2/(4\pi)$, $\lambda = c/\nu$) is exposed for a time Δt

$$P_\nu = \frac{G\lambda^2}{4\pi} \frac{\epsilon_\nu^2}{Z_0\, \Delta t},$$

where $Z_0 = 1/(\varepsilon_0\, c)$ is the intrinsic impedance of free space.

The variance of an electric field can be computed from its spectrum by

$$\sigma_E^2 = \frac{1}{\Delta t} \int_{t_0}^{t_0 + \Delta t} dt\, E^2(t) = \frac{1}{\Delta t} \int_{-\infty}^{+\infty} d\nu\, E_\nu^2,$$

where E_ν is the Fourier transform of $E(t)$ restricted to the time window $[t_0, t_0 + \Delta t]$. E_ν is defined for positive and negative frequencies, while ϵ_ν is a positive-frequency quantity such that $\epsilon_\nu^2 = E_\nu^2 + E_{-\nu}^2$. For the sky noise, this gives

$$\sigma_{\text{sky}}^2 = \frac{1}{\Delta t} \int_0^{+\infty} d\nu\, \epsilon_\nu^2 = \frac{550 \text{ (V/m)}^2}{(a + 1)G} \left[\left(\frac{\nu}{55 \text{ MHz}}\right)^{a+1}\right]_0^{\nu_{\max}},$$

where the sky temperature quoted in Ref. [12] ($T_{sky} \propto \nu^{a-2}$, $a = -0.5$ and $T_{sky}(55\text{ MHz}) = 4800$ K) is used and an upper bound ν_{max} is set to the ν integral. For $G = 1$ and assuming an observational upper bound $\nu_{max} = 80$ MHz we get

$$\sigma_{sky} \approx 30 \ \mu\text{V/m}.$$

References

[1] H. Falcke et al, Nature 435 (2005) 313.

[2] D. Ardouin et al, Nucl. Instrum. Meth. A 555 (2005) 148.

[3] H.R. Allan, in: J.G. Wilson and S.A. Wouthuysen (Eds), Progress in elementary particle and cosmic ray physics, North Holland, 1971, p. 169.

[4] T. Huege, H. Falcke, A& A 412 (2003) 19; T. Huege, H. Falcke, A& A 430 (2005) 779.

[5] O. Scholten, K. Werner, and F. Rusydi, Astropart. Phys. 29 (2008) 94. See also K. Werner, O. Scholten, Astropart. Phys. 29 (2008) 393.

[6] T. Huege, H. Falcke, Astropart. Phys. 24 (2005) 116.

[7] T. Huege, R. Ulrich, R. Engel, Astropart. Phys. 27 (2007) 392.

[8] F.D. Kahn, I. Lerche, Proc. Royal Soc. London A 289 (1966) 206.

[9] T. Gousset, O. Ravel, and C. Roy, Astropart. Phys. 22 (2004) 103.

[10] D. Ardouin et al, Astropart. Phys. 26 (2006) 341.

[11] T. Gousset, J. Lamblin, and S. Valcares, contribution to the 30th International Cosmic Ray Conference, Merida, Mexico, July 2007.

[12] H. Falcke, P. Gorham, Astropart. Phys. 19 (2003) 477.

[13] J. Lamblin, O. Ravel, C. Medina, Internal report SUBATECH, 03/2005.

[14] T. Stanev, High energy cosmic rays, Springer, 2004.

[15] T. Gaisser, Cosmic rays and particle physics, Cambridge University Press, 1990.

[16] J.D. Kraus, Antennas, McGrawHill, 1988.